

New structure candidates for the experimentally synthesized heptazine-based and triazine-based two dimensional graphitic carbon nitride

Luneng Zhao^{#,1,2}, Xizhi Shi^{#,1,2}, Jin Li^{1,2,*}, Tao Ouyang^{1,2}, Chunxiao Zhang^{1,2}, Chao Tang^{1,2}, Chaoyu He^{1,2,†} and Jianxin Zhong^{1,2}

¹Hunan Key Laboratory of Micro-Nano Energy Materials and Devices, Xiangtan University, Hunan 411105, P. R. China

²Laboratory for Quantum Engineering and Micro-Nano Energy Technology and School of Physics and Optoelectronics, Xiangtan University, Hunan 411105, P. R. China

The widely used structure model for both heptazine-based and triazine-based two-dimensional graphitic carbon nitride ($\text{g-C}_3\text{N}_4$) is the flat P-6m2 structure. However, the experimentally synthesized $\text{g-C}_3\text{N}_4$ possess thickness ranging in 0.2-0.5 nm, indicating that the theoretically used flat P-6m2 configurations are not correct ground states. In this work, we propose three new corrugated structures P321, P3m1 and Pca21 with energies of about 65 meV/atom, 70 meV/atom and 74 meV/atom lower than those of the corresponding flat P-6m2, respectively. These corrugated structures have very similar periodic patterns with the flat P-6m2 ones and they are difficult to be distinguished from their top-views. The optimized thicknesses of the three corrugated structures ranging in 1.347-3.142 Å are in good agreement with the experimental results. The first-principles results show that these corrugated structure candidates are also insulators with band gaps slightly larger than those calculated based on the flat P-6m2 model. Furthermore, they also possess suitable band edge positions for sun-light-driven water-splitting at both $\text{pH} = 0$ and $\text{pH} = 7$ environment as the widely used P-6m2. Our results show that these three new structures are more promising candidates for the experimentally synthesized $\text{g-C}_3\text{N}_4$.

PACS numbers:

I. INTRODUCTION

The two-dimensional (2D) graphitic carbon nitride ($\text{g-C}_3\text{N}_4$) is a fascinating conjugated polymer widely used as metal-free photocatalyst for sun-light-driven water-splitting in the arena of solar energy conversion and environment remediation¹⁻³. It is reported that $\text{g-C}_3\text{N}_4$ possesses excellent photocatalytic activities exceeding than the widely used nitrogen-doped TiO_2 ⁴ and $\text{g-C}_3\text{N}_4$ have attracted widespread concern^{1,5}. Many experimental works^{1,6-9} have successfully synthesized the single-layered $\text{g-C}_3\text{N}_4$ and confirmed that they are better than their three-dimensional (3D) counterparts for photocatalytic applications. However, the structural details of the 2D $\text{g-C}_3\text{N}_4$ are still unfixed. Previous literatures¹⁰⁻¹³ have reported that at least seven types of 2D $\text{g-C}_3\text{N}_4$ can be constructed and four of them are related to segments of triazine (C_3N_3) and heptazine (C_6N_7)^{14,15}, with both hexagonal (P-6m2) and orthogonally (Pmc21) assembling manners. The heptazine-based $\text{g-C}_3\text{N}_4$ in both P-6m2 and Pmc21 configurations possess relatively larger nitrogen pores in comparison with the triazine-based ones and they are more stable than the corresponding triazine-based systems in energy¹⁰⁻¹³. At present time, the flat P-6m2 models with energies slightly smaller than the flat Pmc21 ones are considered as the ground states for both the triazine-based and heptazine-based $\text{g-C}_3\text{N}_4$ and they are widely-used as the structure candidates for the synthesized triazine-based¹⁶ and heptazine-based¹⁷ $\text{g-C}_3\text{N}_4$.

Based on the flat P-6m2 model, many theoretical works¹⁸⁻²² have been performed to investigate the fundamental properties and potential applications of 2D $\text{g-C}_3\text{N}_4$. Most of the calculated properties based on such a flat P-6m2 model can match the experimental results well. However, there are obvious evidences to show that the experimentally synthesized $\text{g-C}_3\text{N}_4$ possess thickness in the range of 0.2-0.5 nm^{6,8}, indicating that the flat P-6m2 configurations may not be the configurations

observed in experiments. Therefore, it of great importance to identify the true configurations of the experimentally synthesized $\text{g-C}_3\text{N}_4$. In fact, some previous theoretical works have considered using the corrugated structures to do their researches²³⁻²⁷. Proper atomic corrugations can release energies to make the systems more stable than the exactly flat ones. However, these fragmented works are lack of in-depth understanding of the structural details for the experimentally synthesized 2D $\text{g-C}_3\text{N}_4$. We have also noticed that some low-energy corrugated configurations^{28,29} have been previously proposed for 3D $\text{g-C}_3\text{N}_4$, but these corrugated configurations have not been translated to 2D conditions. Therefore, to systematically investigate the possible corrugated configurations for both the triazine-based $\text{g-C}_3\text{N}_4$ and heptazine-based $\text{g-C}_3\text{N}_4$ are still interesting and necessary work to understand the structure of 2D $\text{g-C}_3\text{N}_4$.

In this work, we report our discovery of three low-energy corrugated configurations P321, P3m1 and Pca21 for the triazine-based and heptazine-based $\text{g-C}_3\text{N}_4$. They possess energies of about 65 meV/atom, 70 meV/atom and 74 meV/atom lower than that of the corresponding flat P-6m2, showing excellent energetic stabilities. We notice that these three new structures and the flat P-6m2 one possess very similar periodic patterns and they are difficult to be distinguished from their top-views. Furthermore, their thicknesses are in the range of 1.347-3.142 Å, which are in good agreement with the experimental results. The first-principles calculations indicate that they are also insulators with energy band gaps just slightly larger than that of the flat P-6m2 one. Their calculated band edges suggest that they are also excellent materials for sun-light-driven water-splitting at both $\text{pH} = 0$ and $\text{pH} = 7$ environment, comparable to the widely used P-6m2. In view of their excellent stabilities, proper thicknesses and electronic properties, we suggest that they are promising candidate structures for the experimentally synthesized $\text{g-C}_3\text{N}_4$.

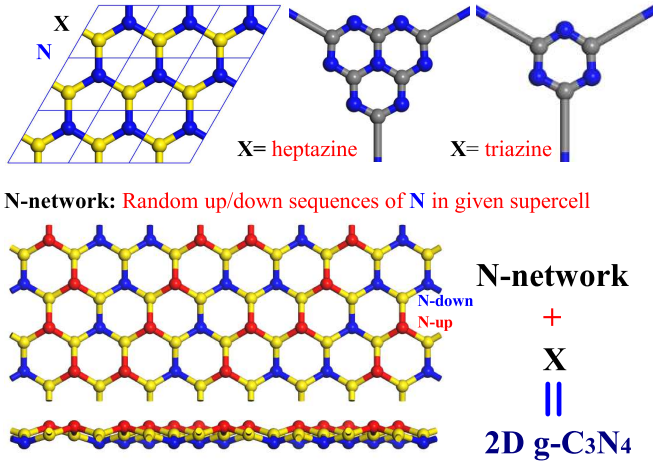


FIG. 1: Sketch map for constructing corrugated configurations of 2D g-C₃N₄. Heptazine and triazine are considered as a three-coordinated super-atoms (X) to insert in the given three-connected binary network NX with different up and down sequences of N atoms, where N indicates the nitrogen atoms.

II. METHODOLOGIES

The widely used P-6m2 structure of the triazine-based and heptazine-based g-C₃N₄ are isomorphic to a hypothetical binary network NX (same as the crystal structure of hexagonal boron nitride), in which X is a hypothetical super-atom for indicating triazine or heptazine, and N indicates the nitrogen atoms as shown in Fig. 1. We notice that to search possible corrugated configurations for 2D g-C₃N₄ is equal to search up and down sequences of N atoms in the hypothetical NX networks. Such a task can be quickly performed by our previously developed RG² code^{30–32}. RG² code is a high-efficient code for generating crystal structures with well-defined structural-feature^{33–37} and it quickly provide us many inequivalent NX networks with different up and down sequences of N atoms and only six-member rings. Associated by an additional small program, the X atoms in these hypothetical NX networks are replaced by triazine or heptazine to construct real corrugated structures for g-C₃N₄. Finally, the structures and stabilities of a series corrugated g-C₃N₄ structures with atoms no more than 56 are further investigated by first-principles calculations. The low-energy P321, P3m1 and Pca21 are further investigated by the high-level HSE06 method on their electronic properties.

In this work, all first-principles calculations are performed by the density functional theory based Vienna Ab initio Simulation Package (VASP)³⁸. The interactions between nucleus and the corresponding valance electrons are described by the projector augmented wave methods (PAW)^{39,40}. Interactions between valance electrons and the exchange-correlation energies are considered through the generalized gradient approximation (GGA) developed by Perdew, Burke, and Ernzerhof (PBE)⁴¹. A plane wave basis with cutoff energy of 500 eV is used to expand the wave functions for all carbon systems

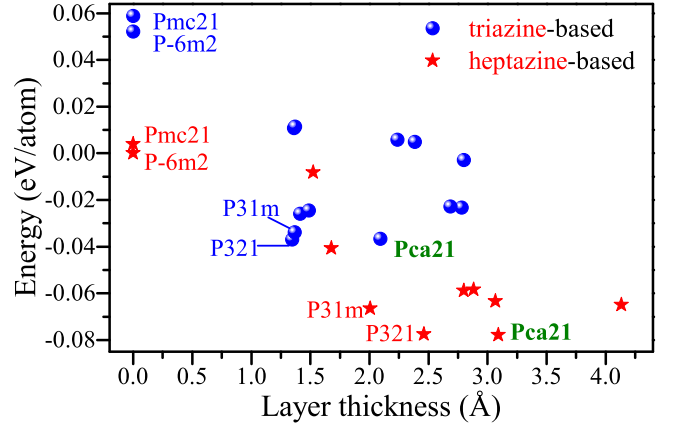


FIG. 2: The calculated total energies of the corrugated g-C₃N₄ and their corresponding layer-thicknesses. The widely-used flat P-6m2 and the three new corrugated P321, P3m1 and Pca21 for both triazine-based and heptazine-based g-C₃N₄ are marked.

and the Brillouin zone sampling meshes are set to be dense enough to ensure the convergence. All the 2D systems are fully optimized until the residual forces on every atom is less than 0.001 eV/Å. The convergence criterion of total energy is set to be 10⁻⁷ eV and the thickness of the slab-model is set to be larger than 15 Å to avoid spurious interactions between adjacent images in our calculations. The high-level HSE06⁴² method is considered to investigate the electronic properties of the three low-energy configurations of g-C₃N₄.

III. RESULTS AND DISCUSSIONS

A. Structures and stabilities

After optimized by first-principles calculations, the calculated total energies of the new corrugated g-C₃N₄ are plotted in Fig. 2 together with their corresponding layer-thicknesses. We can see that all these corrugated configurations are energetically more stable than the corresponding flat P-6m2 ones, indicating that the previously used P-6m2 configurations are not the ground states. It is clear that there are three structures showing excellent energetic stabilities in Fig.2 for both triazine-based and heptazine-based g-C₃N₄. We record them as P321, P3m1 and Pca21 according to their hexagonal and orthogonal symmetries, respectively. As shown in Fig. 3, the corrugated P321, P3m1 and Pca21 are of about 65 meV/atom, 70 meV/atom and 74 meV/atom lower than that of the corresponding P-6m2 configurations, respectively. Their optimized crystal structures are shown in Fig.3 in both top and side views. In fact, P321 and P3m1 are two different reconstructions of the hexagonal $\sqrt{3} \times \sqrt{3}$ supercell ($\frac{\sqrt{3}, 0, 0}{0, \sqrt{3}, 0}$) of P-6m2, and Pca21 is another reconstruction of P-6m2 in its orthogonal supercell ($\frac{2, 1, 0}{0, 1, 0}$), as indicated in Fig. S1.

As shown in Fig. 3, the lattice constants of the optimized P321 ($a=b=11.792$ Å or 7.085 Å), P3m1 ($a=b=11.898$ Å

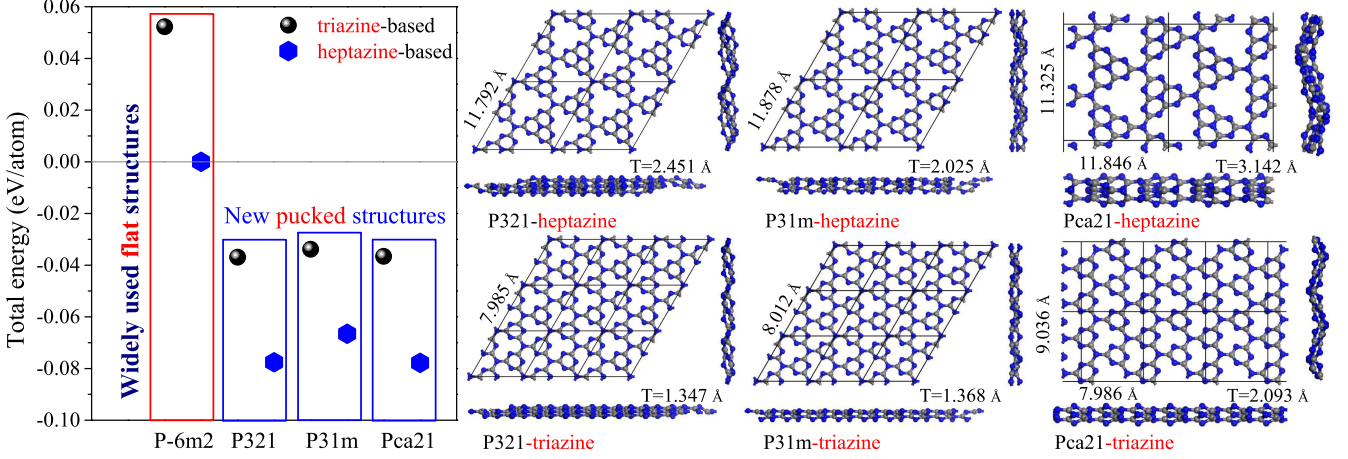


FIG. 3: The calculated total energies of the triazine-based and heptazine-based $g\text{-C}_3\text{N}_4$ in flat P-6m2 configuration and corrugated P321, P3m1 and Pac21 configurations. The optimized crystal structures of the corrugated P321, P3m1 and Pac21 for both triazine-based and heptazine-based $g\text{-C}_3\text{N}_4$ shown in top and side views with corresponding lattice constants and layer-thicknesses.

or 8.012 Å) and Pca21 ($a=11.846$ Å or 9.036 Å, $b=11.325$ Å or 7.986 Å) are very close to those of the corresponding supercells based on the flat P-6m2 model (primitive cell: $a=b=7.135$ Å or 4.785 Å; hexagonal super cell: $a=b=12.362$ Å and 8.290 Å; orthogonal supercell: $a=12.362$ Å or 8.290 Å, $b=12.358$ Å or 8.288 Å). We can see that the top view patterns of the three corrugated configurations are the same as those of the flat P-6m2 structures, showing very similar periotic patterns. Thus, it is difficult to distinguish these structures in experiment from their top views. This may be an important reason that previous researchers consider using the flat P-6m2 model as the structural candidate for the experimentally synthesized $g\text{-C}_3\text{N}_4$. It is interesting that the layer-thicknesses of the three low-energy configurations P321, P3m1 and Pca21 are 1.347 Å (2.451 Å), 1.368 Å (2.019 Å) and 2.093 Å (3.142 Å) for triazine-based (heptazine-based) $g\text{-C}_3\text{N}_4$, respectively. These results show that the new corrugated structures are more consistent with the experimental observation^{6,8}.

B. Electronic properties

We then investigate the electronic properties of these three low-energy $g\text{-C}_3\text{N}_4$ through the high-level HSE06 method and compare them with those of the widely used flat P-6m2. The calculated band structures of both the triazine-based and heptazine-based $g\text{-C}_3\text{N}_4$ in the flat P-6m2 and the corrugated P321, P3m1 and Pac21 configurations are shown in Fig. S2. The results show that the heptazine-based $g\text{-C}_3\text{N}_4$ in flat P-6m2 is a semiconductor with indirect band gap of 2.77 eV and the triazine-based one possesses direct band gap of about 3.184 eV. These results are good agreement with the previously reported experimental¹ and theoretical values¹⁰, which confirm that our used methods are reliable.

As discussed before, proper atomic corrugations will release corresponding energies to make the systems more en-

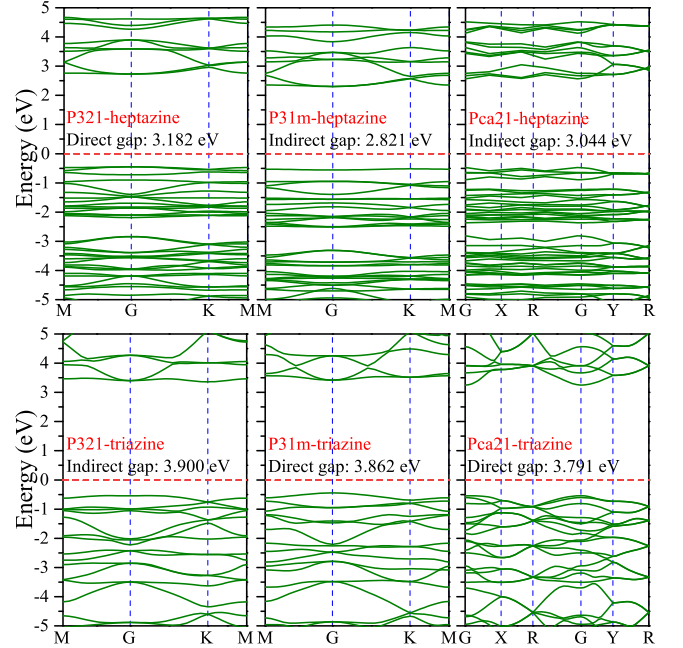


FIG. 4: The electron band structures of the triazine-based and heptazine-based $g\text{-C}_3\text{N}_4$ in configurations the corrugated P321, P3m1 and Pac21 calculated from HSE06 methods. The corresponding band gaps and types are also inserted.

ergetically stable. Here, we can see that these corrugations (P321, Pm31 and Pca21) will also enlarge the band gaps of the systems to enhance their chemical stabilities. As the band structures of the heptazine-based $g\text{-C}_3\text{N}_4$ shown in Fig. 4, we can see that the splitting energies between the bonding and anti-bonding orbits are enlarged due to the atomic corrugations. The band gaps of the heptazine-based $g\text{-C}_3\text{N}_4$ in

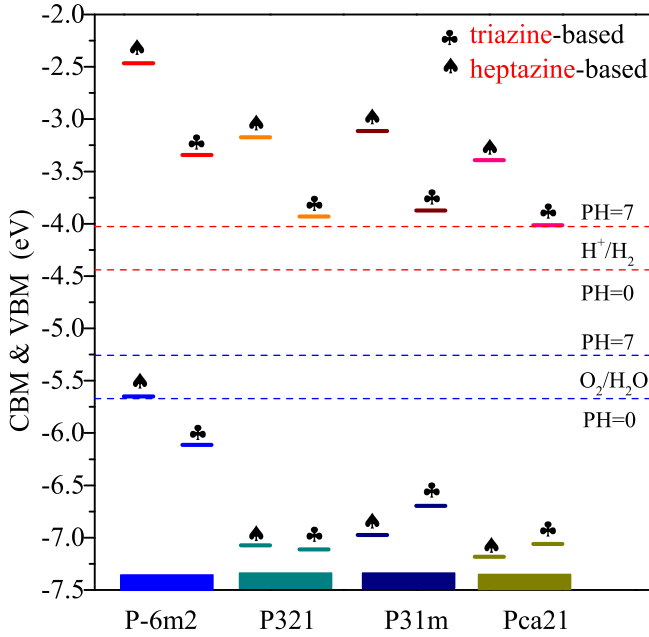


FIG. 5: The HSE06-based CBM and VBM positions of the triazine-based and heptazine-based $g\text{-C}_3\text{N}_4$ in configurations of flat P-6m2 and corrugated P321, P3m1 and Pca21 with respect to the redox potentials for water splitting at $pH = 0$ and $pH = 7$ situations.

the corrugated P321, P3m1 and Pca21 are correspondingly increased to be 3.182 eV, 2.821 eV and 3.044 eV, respectively. For the triazine-based $g\text{-C}_3\text{N}_4$, the band gaps of the corrugated P321, P3m1 and Pca21 are also enlarged to be 3.90 eV, 3.862 eV and 3.791 eV, respectively. These increased splitting energies or band gaps between the bonding and anti-bonding orbits can help us to understand the corrugation-induced energy release in the systems. Furthermore, it is found that the amplifications of band gaps between flat and corrugated $g\text{-C}_3\text{N}_4$ are relatively small. For heptazine-based $g\text{-C}_3\text{N}_4$, the amplifications of band gaps induced by corrugations in P321, P3m1, Pca21 are 0.412 eV, 0.051 eV and 0.274 eV, respectively. For the triazine-based $g\text{-C}_3\text{N}_4$, these amplifications are 0.816 eV, 0.678 eV and 0.607 eV. That is to say, previous literatures can use the calculated band gaps based on the flat P-6m2 model to explain the experimental values well, no matter the experimentally synthesized $g\text{-C}_3\text{N}_4$ is the flat P-6m2 or the corrugated P321, P3m1 and Pca21.

Another important feature of the experimentally synthesized $g\text{-C}_3\text{N}_4$ is the exotic properties for metal-free photocatalysis. Based on the flat P-6m2 models, the excellent potentials of $g\text{-C}_3\text{N}_4$ for sun-light-driven water-splitting have been well understood by their CBM and VBM positions satisfying the redox potentials of the water splitting^{10,20,23,25,27}. We think this is another important reason why the flat P-6m2 models are considered as structure candidates for the experimentally synthesized $g\text{-C}_3\text{N}_4$. Here, we show that the low-energy P321, P3m1 and Pca21 are also excellent materials for metal-free sun-light-driven water-splitting. As shown in Fig.5, the

HSE06-based CBM and VBM positions of the triazine-based and heptazine-based $g\text{-C}_3\text{N}_4$ in configurations of flat P-6m2 and corrugated P321, P3m1 and Pca21 are arranged together with the redox potentials for water splitting at $pH = 0$ and $pH = 7$ situations. For both $pH = 0$ and $pH = 7$ situations, all the CBM positions of the corrugated configurations located slightly above the reduction potential of H^+/H_2 . And the corresponding VBM positions are also lower than the reduction potential of $\text{O}_2/\text{H}_2\text{O}$. These band edge positions of the three new corrugated configurations suggest that they are also appropriate for sun-light-driven water splitting in both acidic and neutral situations.

Above results and discussions can help us to understand why the flat P-6m2 models are widely used as the crystal structures for the experimentally synthesized $g\text{-C}_3\text{N}_4$ in previous literatures. We think that the most important reason is that there is no any optional structure to use. The widely-used flat P-6m2 models can be accepted as the correct structures due to the facts that their surface topographies (top views), electronic properties (band gaps) and potentials in sun-light-driven water-splitting (band edge positions) are very similar to those of the experimentally synthesized corrugated structures. It is still difficult to say what is the true configurations for the corrugated 2D $g\text{-C}_3\text{N}_4$ at present time. Maybe the structure morphologies of the synthesized 2D $g\text{-C}_3\text{N}_4$ are substrate-dependent. The three new corrugated configurations are promising candidates in views of their excellent stabilities, proper thicknesses and electronic properties.. We believe that the orthogonal Pca21 configurations are the most possible candidates according to their lowest energies. We have also show that they are dynamically stable according to the simulated vibrational spectrum as shown in Fig. S3.

IV. CONCLUSION

In summary, three corrugated configurations P321, P3m1 and Pca21 were proposed as new candidate structures for the experimentally synthesized $g\text{-C}_3\text{N}_4$. The first-principles calculations show that these three new configurations are more energetically favorable than the flat P-6m2 models. These three corrugated configurations possess similar periodic patterns with those of flat P-6m2 models. However, the corrugated P321, P3m1 and Pca21 with certain layer-thicknesses are more suitable for explaining the thicknesses of the experimentally synthesized $g\text{-C}_3\text{N}_4$. The calculated band gaps of the corrugated P321, P3m1 and Pca21 are also close to those calculated based on the flat P-6m2, which can further help us to understanding the previous belief of using the P-6m2 model. Furthermore, the band edge positions of these three new corrugated configurations for both triazine-based and heptazine-based $g\text{-C}_3\text{N}_4$ are also appropriate for sun-light-driven water-splitting in both acidic and neutral situations. Our results show that these three new corrugated configurations are promising structure candidates for the experimentally synthesized single layer of $g\text{-C}_3\text{N}_4$.

V. ACKNOWLEDGEMENT

This work is supported by the National Natural Science Foundation of China (Grants No. 11974300, 11974299, 11704319 and 11874316), the Natural Science Foundation

of Hunan Province, China (Grant No. 2016JJ3118 and 2019JJ50577), and the Program for Changjiang Scholars and Innovative Research Team in University (No. IRT13093).

These authors contributed equally to this work.

-
- * Electronic address: lijin@xtu.edu.cn
 † Electronic address: hechaoyu@xtu.edu.cn
- ¹ X. C. Wang, K. Maeda, A. Thomas, K. Takanabe, G. Xin, J. M. Carlsson, K. Domen and M. Antonietti, *Nat. Mater.*, **8**, 76, (2009).
 - ² A. J. Du, S. Sanvito, Z. Li, D. W. Wang, Y. Jiao, T. Liao, Q. Sun, Y. H. Ng, Z. H. Zhu, R. Amal and S. C. Smith, *J. Am. Chem. Soc.*, **134**, 4393 (2012).
 - ³ J. S. Zhang, Y. Chen and X. C. Wang, *Energy Environ. Sci.*, **8**, 3092 (2015).
 - ⁴ S. C. Yan, Z. S. Li and Z. G. Zou, *Langmuir*, **25**, 10397 (2009).
 - ⁵ W. J. Ong, L. L. Tan, Y. H. Ng, S. T. Yong and S. P. Chai, *Chem. Rev.*, **116**, 7159 (2016).
 - ⁶ Y. Chen, B. Wang, S. Lin, Y. Zhang and X. Wang, *J. Phys. Chem. C*, **118**, 29981 (2014).
 - ⁷ H. Zhao, H. Yu, X. Quan, S. Chen, H. Zhao and H. Wang, *RSC Adv.*, **4**, 624 (2014).
 - ⁸ J. Xu, L. Zhang, R. Shi and Y. Zhu, *J. Mater. Chem. A*, **1**, 14766 (2013).
 - ⁹ H. Zhao, H. Yu, X. Quan, S. Chen, Y. Zhang and H. Zhao, *H. Wang, Appl. Catal. B: Environ.*, **152**, 46 (2014).
 - ¹⁰ P. L. Sun, C. Y. He, C. X. Zhang, H. P. Xiao and J. X. Zhong, *Physica B*, **562**, 131 (2019).
 - ¹¹ Y. Zheng, L. Lin, B. Wang and X. Wang, *Angew. Chem., Int. Ed.* **2015**, **54**, 12868.
 - ¹² E. Kroke, M. Schwarz, E. Horath-Bordon, P. Kroll, B. Noll and A. D. Norman, *New J. Chem.*, **26**, 508 (2002).
 - ¹³ X. G. Ma, Y. H. Lv, J. Xu, Y. F. Liu, R. Q. Zhang and Y. F. Zhu, *J. Phys. Chem. C*, **116**, 23485 (2012).
 - ¹⁴ A. Zambon, J. M. Mouesca, C. Gheorghiu, P. A. Bayle, J. Pecaut, M. Claeys-Bruno, S. Gambarelli and L. Dubois, *Chem. Sci.*, **7**, 945 (2016).
 - ¹⁵ Y. Zhao, J. Zhang and L. Qu, *ChemNanoMat*, **1**, 298 (2015).
 - ¹⁶ G. Algara-Siller, N. Severin, S. Y. Chong, T. Björkman, R. G. Palgrave, A. Laybourn, M. Antonietti and Y. Z. Khimyak, *Angew. Chem. Int. Ed.*, **1**, 53 (2014).
 - ¹⁷ S. B. Yang, Y. J. Gong, J. S. Zhang, L. Zhan, L. L. Ma, Z. Y. Fang, R. Vajta, X. C. Wang and P. M. Ajayan, *Adv. Mater.*, **25**, 2452 (2013).
 - ¹⁸ H. Basharnavaz, A. Habibi-Yangjeh and M. Mousavi, *Appl. Surf. Sci.*, **456**, 882 (2018).
 - ¹⁹ X. Zhi, Y. Jiao, Y. Zheng and S. Z. Qiao, *Small*, **15**, 1804224 (2019).
 - ²⁰ X. Ma, Y. Lv, J. Xu, Y. Liu, R. Zhang and Y. Zhu, *J. Phys. Chem. C*, **116**, 23485 (2012).
 - ²¹ I. Choudhuri, G. Bhattacharyya, S. Kumar and B. Pathak, *J. Mater. Chem. C*, **4**, 11530 (2016).
 - ²² T. Hussain, M. Hankel and D. J. Searles, *J. Phys. Chem. C*, **120**, 25180 (2016).
 - ²³ C. J. Ren, Y. L. Zhang, Y. L. Li, Y. F. Zhang, S. P. Huang, W. Lin and K. N. Ding, *J. Phys. Chem. C*, **123**, 17296 (2019).
 - ²⁴ Q. Gao, H. L. Wang, L. F. Zhang, S. L. Hu and Z. P. Hu, *Front. Phys.*, **13**, 138108 (2018).
 - ²⁵ X. Chen, X. Zhao, Z. Kong, W. J. Ong and N. Li, *J. Mater. Chem. A*, **6**, 21941 (2018).
 - ²⁶ J. Sun, X. Li and J. Yang, *Nanoscale*, **10**, 3738 (2018).
 - ²⁷ L. M. Azofra, D. R. MacFarlane and C. Sun, *Phys. Chem. Chem. Phys.*, **18**, 18507 (2016).
 - ²⁸ J. Gracia and P. Kroll, *J. Mater. Chem.*, **19**, 3013 (2009).
 - ²⁹ C. J. Pickard, A. Salamat, M. J. Bojdys, R. J. Needs and P. F. McMillan, *Phys. Rev. B*, **94**, 094104 (2016).
 - ³⁰ H. C. Yin, X. Z. Shi, C. Y. He, M. Martinez-Canales, J. Li, C. J. Pickard, C. Tang, T. Ouyang, C. X. Zhang, and J. X. Zhang, *Phys. Rev. B*, **99**, 041405(R) (2019).
 - ³¹ X. Z. Shi, C. Y. He, C. J. Pickard, C. Tang, and J. X. Zhong, *Phys. Rev. B*, **97**, 014104 (2018).
 - ³² C. Y. He, X. Z. Shi, S. J. Clark, J. Li, C. J. Pickard, T. Ouyang, C. X. Zhang, C. Tang, and J. X. Zhong, *Phys. Rev. Lett.*, **121**, 175701 (2018).
 - ³³ P. L. Sun, C. Y. He, C. X. Zhang, H. P. Xiao and J. X. Zhong, *Physica B: Condens. Matt.*, **562**, 131 (2019).
 - ³⁴ N. Jiao, P. Zhou, C. Y. He, J. J. He, X. L. Liu and L. Z. Sun, *Phys. Status. Solidi-RRL*, **13**, 1900470 (2019).
 - ³⁵ Z. Q. Li, X. Z. Shi, C. Y. He, T. Ouyang, J. Li, C. X. Zhang, S. F. Zhang, C. Tang, R. A. Roemer and J. X. Zhong, *Appl., Surf. Sci.*, **497**, 143803 (2019).
 - ³⁶ N. Zhou, P. Zhou, J. Li, C. Y. He and J. X. Zhong, *Phys. Rev. B*, **100**, 115425 (2019).
 - ³⁷ X. Yang, C. Y. He, X. Z. Shi, J. Li, C. X. Zhang, C. Tang and J. X. Zhong, *J. Appl. Phys.*, **124**, 163107 (2018).
 - ³⁸ G. Kresse, and J. Furthmüller, *Phys. Rev. B*, **54**, 11169 (1996).
 - ³⁹ P. E. Blöchl, *Phys. Rev. B*, **50**, 17953 (1994).
 - ⁴⁰ G. Kresse, and D. Joubert, *Phys. Rev. B*, **59**, 1758 (1999).
 - ⁴¹ J. P. Perdew, K. Burke, and M. Ernzerhof, *Phys. Rev. Lett.*, **77**, 3865 (1996).
 - ⁴² J. Heyd, G. E. Scuseria, M. Ernzerhof, *J. Chem. Phys.*, **118**, 8207 (2003).